DOI: 10.1002/minf.200

# Simultaneous prediction of four ATP-binding cassette transporters substrates using multi-label QSAR

Natália Aniceto[a], Alex Freitas[b], Andreas Bender[c], Taravat Ghafourian[a,d]*

**Abstract:** Efflux by the ATP-binding cassette (ABC) transporters affects the pharmacokinetic profile of drugs and it has been implicated in drug-drug interactions as well as its major role in multi-drug resistance in cancer. It is therefore important for the pharmaceutical industry to be able to understand what phenomena rule ABC substrate recognition. Considering a high degree of substrate overlap between various members of ABC transporter family, it is advantageous to employ a multi-label classification approach where predictions made for one transporter can be used for modeling of the other ABC transporters. Here, we present decision tree-based QSAR classification models able to simultaneously predict substrates and non-substrates for BCRP1, P-gp/MDR1 and MRP1 and MRP2, using a dataset of 1493 compounds. To this end, two multi-label classification QSAR modelling approaches were adopted: Binary Relevance (BR) and Classifier Chain (CC). Even though both multi-label models yielded similar predictive performances in terms of overall accuracies (close to 70%), the CC model overcame the problem of skewed performance towards identifying substrates compared with non-substrates, which is a common problem in the literature. The models were thoroughly validated by using external testing, applicability domain and activity cliffs characterization. In conclusion, a multi-label classification approach is an appropriate alternative for the prediction of ABC efflux.

**Keywords:** Multi-label Classification, QSAR, transporter, P-glycoprotein, Multidrug-resistance Associated Protein, Breast Cancer Resistance protein, BCRP1, MRP1, MRP2

## 1 Introduction

The drug development process is becoming increasingly more expensive over the years, which is partly caused by stricter testing demanded by regulatory entities for a drug to be accepted into the market. At the same time the reduction of animal experimentation has become a priority. As a result in silico programs in the pharmaceutical industry play an increasingly important role in drug discovery for the financial sustainability of a company.

The ATP-binding cassette (ABC) family is composed (in humans) of 48 exclusive membrane exporters that are grouped in seven families (ABCA-G) according to gene similarity with respect to sequence and organization. They transport a wide variety of endogenous and exogenous compounds, which range from ions to macromolecules, via an ATP-dependent mechanism.[1-2] These transporters are highly expressed in a variety of tissues, among which are some important distribution barriers that are associated with drug absorption and distribution impairment. Some examples are the intestinal brush border membrane, the blood-brain barrier, and the hepatocytic biliary canalicular membrane.[3] The role of membrane transporters in absorption, distribution and excretion as well as the possible drug interaction due to binding to these transporters indicate the importance of membrane transporters to drug discovery and development, where about 1/3 of the attrition rate in drug development is caused by a poor pharmacokinetic profile.[4] Something as simple as a high hepatic clearance can render the use of a highly active, non-toxic drug unfeasible due to the need for very short dosage periods. Properties like this are often not discovered until human trials, which means that any drug withdrawals are extremely expensive for the company. *In silico* studies are a promising and inexpensive tool to avoid or at least minimize late drug attrition rate. Among these, quantitative structure-activity (or property) relationships (QSAR) have long been implemented in the drug discovery and development process.

Given the high potential of ABC transporters for pharmacoketic impact and also their potential for drug-drug interaction, these membrane transporters are one of the most important targets that need to be studied during drug discovery. In addition, some ABC transporters including the Breast Cancer Resistance Protein (BCRP1, ABCG2), P-glycoprotein (P-gp, MDR1, ABCB1), and the Multidrug Resistance-associated Proteins (MRP1-7, ABCC1-6 and 10)[1] are strongly associated with multi-drug resistance in cancer cells given their ability to extrude drugs from the cell.[2] QSAR appears to be a particularly well suited method to predict ABC transport substrates since it has been shown that substrate recognition by the aforementioned ABC members relies on global physicochemical profiles rather than following the key-and-lock ligand binding model.[2] The potential of QSAR to predict ABC transporter substrates during the R&D process has already been demonstrated by Desai et al.[5] who reported the successful replacement of an *in vitro* automated assay with a QSAR model to predict P-gp substrates in an early stage of the drug development pipeline of Eli Lilly. Currently, improving the accuracy of QSARs to predict (classify) substrates and non-substrates of ABC transporters remains a challenge. This is partly due to the multi-specific nature of the substrate recognition by these transporters. Different ABC family members have shown redundancy in terms of substrate recognition and transport,[2, 6] and in order to take advantage of this, we suggest a multi-label QSAR approach to address the ABC transport as a whole, as opposed to the traditional single-label QSAR approach looking at each transporter individually.

In traditional supervised learning, among *n* training instances (compounds in the dataset), each instance (compound) is assumed to be associated with a single response (called label). In other words, in a single-label classifier, each compound is classed under one label (response), e.g. active or inactive. So for each response (label), a different classifier is produced which is independent from the classifier produced for other labels.[7] However, there are cases where instances, due to their complexity, might have various simultaneous responses, which is the same as saying that an instance is associated to a set of various labels rather than just one. This is the case of the ABC transport problem, where different compounds are effluxed by different types of ABC transporters, and it constitutes a multi-label classification problem. So, in this scenario, the machine learning algorithm produces a multi-label classifier, which can be viewed as a set of single-label classification models, one per label (response).[7-8]

However, one of the big issues in multi-label machine learning is that labels can have interdependency between them[8]. Correlation between labels potentially holds important information about the modelled problem, and accounting for this is crucial in facilitating the learning algorithm[9]. As a result, the main goal in multi-label machine learning is to enable the detection of these relationships. This means that the considerable overlap between substrates (and inhibitors) of various ABC transporters should be exploited from the data mining standpoint to improve the model performance.

Within multi-label classification techniques, one of the most widely used problem transformation methods is Binary Relevance (BR), which decomposes the multi-label problem into a binary problem for each label separately. A regular single-label classifier is then applied to predict the 0/1 class in every separate label ignoring the information from the remaining labels. The separate predictions from all the single-label classification tasks are finally gathered in one multi-label prediction.[8, 10] Consequently, BR has a major drawback by assuming label independence. By separating the labels one is in fact losing potentially useful information and it leads to a situation like predicting impossible coexisting labels in practice.[8, 10] An alternative to this is the classifier chain (CC) method that is able to address label dependency.[10] In this technique, the different labels originating from single-label models communicate the learned information to each other, in a sequential fashion.

A multi-label approach has recently been applied to classify inhibitors/non-inhibitors of two transporters, P-gp and BCRP1 [11], although the authors reported no value in accounting for label overlap for the inhibitors of these two proteins. Here, we have focused instead on the substrates/non substrates of four major ABC transporters, namely BCRP1, MDR1/P-gp, MRP1, MRP2, using novel multi-label classification methods. The goal was to assess the potential value of taking into account the data overlap amongst transporters in terms of the predictive accuracy of the classifier, as well as finding molecular characteristics that are unique to, or those that overlap between the substrates of various transporters. The two previously mentioned multi-label modelling schemes, BR and CC, were employed where the only difference between them is the absence or presence of communication between transporter models, respectively. A comprehensive validation routine including the characterization of the applicability domain (AD) and activity cliffs (AC) were carried out for the models. The predictive performance was analyzed against each model's applicability domain and activity cliff analysis, in the attempt of providing a more holistic, in-depth interpretation of the models' true worth. To our knowledge this is the first reported multi-label classification model for the prediction of ABC substrates (S) and non-substrates (NS), providing insight on transporter relationship with regard to binding patterns.

## 2 Experimental Section

### 2.1 Dataset

A dataset of 1493 compounds was compiled from the substrate data available on the Metrabase database[12] (accessed on October 2014) for six ABC transporters: BCRP1, MDR1, MRP1, MRP2, MRP3 and MRP4. All instances were divided into two classes: substrates and non-substrates. The collection of SMILES provided was checked for repetitions and isomers using ACD Labs, and mixtures were removed. Repetitions were merged and, for cases of conflicting information, the principle of minimum evidence was applied, by which all compounds with at least one case of reported substrate property were regarded as potential substrates and so, they were classified as substrates. This is a valid approach considering that all the initial data collected from Metrabase was selected based on quality standards.[12]

Prior to any modelling or modelling-related task the dataset was submitted to a stratification procedure as described by Sechidis et al.[13]. The authors show that this procedure leads to data subsets with more balanced class label distributions in a series of benchmark datasets. That is, this procedure maximizes transporters distribution across different data partitions. This procedure was implemented in R using the provided pseudo-code. Consequently, the dataset was divided into training (TR), internal validation (IV) and test (TE) set in a proportion of 6:2:2 (895 + 299 + 299 compounds), respectively, with similar distribution of substrates and non-substrates in TR, IV and TE. For larger datasets, i.e. BCRP1, MDR1, MRP1 and MRP2 compounds, there was only a negligible imbalance of data with the substrate (S) to non-substrate (NS) ratio of 1.7, 1.3, 1.0 and 1.2, respectively (see Figure 1). However, for the transporter classes associated with smaller datasets, namely MRP3 and MRP4, the S to NS ratio was around 2.5, which led to insufficient number of non-substrates for modelling and validation. Therefore, these two transporters were eliminated and the remaining four transporters were investigated.

### 2.2 Calculation of Molecular Descriptors.

Molecular descriptors were calculated using ACD/labs logD suite v12.5 and MOE 2013, using the SMILES codes retrieved from Metrabase. Using ACD, prior to molecular descriptors calculation, all structures were submitted to desalting. In MOE, the compounds' structures were washed (counter ions were removed) and minimized. Molecular mechanics minimization was initially performed using MMFF94x, followed by a second minimization using quantum mechanics Self-Consistent Field (SCF), where partial charges were assigned using the PM6 Hamiltonian. The PM6 semi-empirical method was added to MOE as a MOPAC 2009[14] extension. After descriptor calculation, all external, non-variant and mainly zero-valued descriptors (with ≥97% zero values) were removed. No single charge-assignment method was selected over any other, across homologous descriptors, as it has been shown that different charge assignment methods have led to variable success in modelling different datasets in the past.[15] This allows a data-driven selection of charge-related molecular descriptors using PEOE vs PM6 methods, as well as various descriptors derived from semiempirical methods, AM1, PM3 and MNDO.

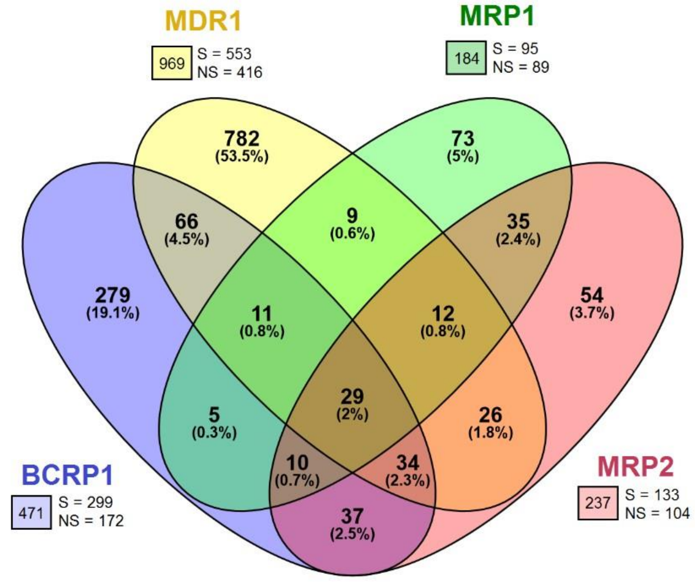

**Figure 1.** Schematic summary of transporter overlap represented in the Venn diagram. Below each transporter label are the total number of instances (in a square) in the full dataset, and the corresponding amount of substrates and non-substrates.

### 2.3 Pre-processing feature selection.

A total of five feature sets derived from five different feature selection techniques were produced for each of the four ABC transporters. Five different feature selection methods were implemented using the popular data mining tool Weka 3.6: three filter methods, namely Genetic Algorithm (GA), Greedy Stepwise search (GS) and ReliefF (RfF); and two wrapper methods, namely C4.5 Decision Tree-Genetic Algorithm (J48-GA) and Random Forest-Greedy Stepwise search (RF-GS). For detailed information on the functioning of filter and wrapper methods please refer to the literature.[16-17] All feature selection methods were run using the TR set only. Filter methods were implemented with CfsSubsetEval attribute evaluator (which selects the subsets of features that are highly correlated with the class while having low intercorrelation), and wrapper methods were implemented with ClassifierSubsetEval (classifier subset evaluator in Weka). For the GA method the following

0.8 and 0.01 crossover and mutation probabilities, and both the population and generation

0.8 and 0.01 crossover and mutation probabilities, and both the population and generations size were set to 100, to allow sufficient exploration of the feature space. GS and RfF were implemented using default settings (with the latter coinciding with previously reported settings)[18].

Within the wrapper methods RF-GS and J48-GA were implemented by combining two search algorithms (GS and GA), respectively, with two classifiers (RF and J48). In J48-GA, the settings for the GA feature searcher were the same as the ones used for the GA filter method. As for the J48 classifier within the wrapper, the pruning method was optimized by 10-fold cross validation. When applicable, the confidence factor was optimized in a range between 0.1 and 0.5 (with a 0.1 step). All other conditions in J48 were set to default values. In the RF-GS method the trees were limited to a maximum depth of 3, as the focus is tree number not tree depth. The number of trees (ranging from 1 to 25) was optimized using the 10-fold cross-validation root-mean squared error.

To minimize local-minima effects that have been particularly reported for GA[19], for all feature selection methods 10-fold cross validation was repeated 5 times using different random seeds, and ranking scores were averaged across the 5 runs. The top 20 features were selected from the average ranking.

### 2.4 Multi-label QSAR models.

Each of the five feature sets obtained from the feature selection routines were subsequently used to train a J48 model (Weka 3.6), for each of the labels (transporters). J48 training used the same parameters as described for the J48-GA feature selection method mentioned above. These models were then tested on an independent internal validation (IV) data subset. This corresponds to a total of 20 experiments testing five different feature sets for each of the four ABC transporters. The best feature set for each transporter was selected according to the highest Matthews correlation coefficient (MCC) and geometric mean between sensitivity and specificity (G-mean) in the IV set.

The best J48 models (using the best feature selection conditions) were selected for each of the training sets (BCRP1=288, MDR1=580, MRP1=111, MRP2=145).

The multi-label BR model was obtained by gathering the predictions from these four best single-label models into one global prediction output. In this case, whenever a new query compound needs to be predicted it would be passed through all four ABC models and a set of label predictions would be produced. For the multi-label CC model, the schematic representation of CC is depicted in Figure 2. The transporters were ordered according to descending order of dataset size, based on the theoretical expectation that larger datasets will have a better chance of providing useful information to smaller datasets than the other way around. Accordingly, the order of the labels in the classifier chain was P-gp/MDR1 > BCRP1 > MRP2 > MRP1. To build the multi-label CC model each label (transporter) in the 4-label chain uses the best descriptor set previously optimized for the BR model. In addition, as it can be seen in Figure 2, each label in the CC model uses prediction sets from previously available labels. In summary, in the CC model every label (transporter) in the chain is trained using the prediction sets from all previous labels, along with a set of molecular descriptors (previously selected). To illustrate this, label #3 for example, will be trained with a set of molecular descriptors as well as class predictions for label #1 and #2

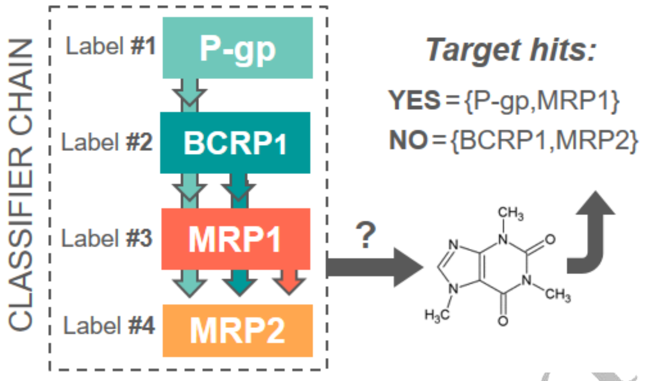

**Figure 2.** Schematic representation of multi-label classifier chain training.

Overall each transporter was submitted to an independent and parallel process of feature selection, model optimization and training, and finally testing. All these steps were performed in parallel on the same datasets for CC and BR in order to: 1) allow comparability between both types of model at every level, and 2) assess the value of addressing the overlap in the data, by fixing all other conditions in both modelling workflows. Throughout the paper the following notation *<single-label model>* - *<multi-label model>* will be used whenever a specific single-label model within the CC or the BR models is mentioned.

**2.5 Model validation** The single-label performance measures used for single-label model assessment are defined below [20], where TP, TN, FP and FN stand for the numbers of true positives, true negatives, false positives and false negatives, respectively. These correspond to Sensitivity (SEN), specificity (SPE), Matthew's correlation coefficient (MCC), and the geometric mean between SEN and SPE (G-mean).

$$SEN = \frac{TP}{TP + FN}$$

$$SPE = \frac{TN}{TN + FP}$$

$$MCC = \frac{TP \times TN - FP \times FN}{\sqrt{(TP + FN) \times (TN + FP) \times (TP + FP) \times (TN + FN)}}$$

$$G - mean = \sqrt{SEN \times SPE}$$

Several multi-label predictive accuracy measures were used, namely the harmonic mean between precision and recall (F1), Precision (P) and Recall (R), calculated according to Tsoumakas and Katakis [21-22]. Hamming Loss (HL) was used solely to monitor the impact of each label on the multi-label model's performance, during model building.

$$Hamming\ Loss = \frac{1}{N} \sum_{;?@}^{>} \frac{|Y_{;} \Delta Z_{;}|}{|L|}$$

$$F1 = \frac{1}{N} \sum_{;?@}^{>} \frac{2|Y_{;} \cap Z_{;}|}{|Z_{;}| + |Y_{;}|}$$

$$P = \frac{1}{N} \sum_{;?@}^{>} \frac{|Y_{;} \cap Z_{;}|}{|Z_{;}|}$$

$$R = \frac{1}{N} \sum_{;?@}^{>} \frac{|Y_{;} \cap Z_{;}|}{|Y_{;}|}$$

In these measures, $Y_i$ and $Z_i$ correspond to the set of observed and predicted labels, respectively, for the *i*-th compound, N corresponds to the number of compounds in the dataset, and L corresponds to the number of modelled labels. The Δ symbol denotes the symmetric difference between two sets of label values (observed and predicted, in this case), which is equivalent to the XOR boolean operation.

As substrates are more frequent than non-substrates in all labels, a balanced accuracy (bACC) was used to take into account this when assessing predictive performance, which consisted of the average G-mean across every label j (which, in turn, can be considered as the single-label balanced accuracy). To evaluate the balance between substrate and non-substrate performances across instances, ΔPR measures the average deviation in precision and recall between substrates and non-substrates.

$$bACC = \frac{1}{L} \sum_{F?@}^{G} \sqrt{SEN_{F} \times SPE_{F}}$$

$$\Delta PR = \frac{(P_{\mathrm{H}} - P_{>\mathrm{H}}) + (R_{\mathrm{H}} - R_{>\mathrm{H}})}{2}$$

### 2.6 Applicability Domain

For any QSAR model, it is necessary to define the domain of applicability to ensure its reliability in the prediction of properties of external compounds. In this study, the applicability domain (AD) of all the single label models used in the generation of multi-label BR and CC models were characterized. To determine the AD, the distance to the model based on the standard deviation (STD) of the predicted values (or labels) from the ensemble of various models was used, as this has been shown to be the most successful method in quantifying predictive reliability across chemical space in the data.[23-27] This technique capitalizes on the concept that the disparity between predictions computed from a group of models (ensemble) is a direct consequence of prediction reliability. A small standard deviation will equate to highly reliable predictions, whereas a larger value signals unreliable predictions. It has been demonstrated that the disagreement between models leads to a better separation between reliable and unreliable predictions compared to traditional structure-based measures.[27]

In this work, J48 models were developed for 10 random samples of training set data, each sample comprising 80% of the training set compounds.

$$STD = \frac{y_{\mathrm{K}} - y^{\mathrm{L}}}{N-1}$$

STD values were calculated for each compound using the equation above. Here, $y_{\mathrm{K}}$ is the class label prediction using model *m* and $y$ is the average of all prediction outputs for this compound by *N* models. For classification models (which is the case here) predictions y take the form of probabilities. By setting increasingly larger STD thresholds (with increments of 0.05), which can also be perceived as increasing distance to the model's reliability core, more compounds become included in the model. By performing this kind of scanning through the model's space, one is able to establish a profile of reliability as a function of STD. In this case we used % correct predictions, the so-called accuracy as our measure of reliability.

### 2.7 Activity cliffs

To search for possible activity cliffs, the similarities between all pairs of compounds were calculated using the well-known Tanimoto coefficient (Tc) applied on 1024 bit Morgan circular fingerprints (equivalent to the extended connectivity fingerprints [ECFP], calculated using the RDkit module in python), for a radius of 2.Following the criteria for activity cliffs used by several authors[28-30], we defined as an activity cliff any substance that has a different class than the majority class of the 3 nearest training neighbors, which must all show a Tc > 0.55 to the analyzed compound. This threshold has been reported as a sensible value above which compounds are visibly similar.[28-30]

### 2.8 Visualization of chemical space

In order to gauge how wide is the chemical space of the built models, with relation to the real-world drug chemical space, the ABC transporter data was overlaid against the DrugBank chemical space. In order to visualize the chemical space coverage, t-Distributed Stochastic Neighbor Embedding (t-SNE)[31] was chosen as the multidimensional scaling technique. This technique is one of the most successful in conserving the multidimensional structure of the data during its projection into a low-dimensional plot.[31] t-SNE was employed over a set of 1024 bit Morgan circular fingerprints (RDKit equivalent of ECFP), calculated for a radius of 2. To compute the t-SNE projection, an implementation in python, provided by the developer (https://lvdmaaten.github.io/tsne/#implementations), was used.

## 3 Results

### 3.1 Multi-label QSAR models

In this work, the main goal was to model four ABC transporters in such a way that allows accounting for possible underlying correlations between labels (*i.e.* transporters). Multi-label classification is the appropriate approach to achieve this. By comparing a multi-label method that takes into account label interaction (i.e., CC) with an alternative method that assumes labels to be independent (i.e. BR) one is able determine whether label interaction, in fact, exists. Both multi-label classifiers were trained using the best features selected by various feature selection methods for each transporter, and they differ only in the use of previous label predictions as additional features (in the case of CC). The rational for the use of multi-label methods was the overlap observed in the dataset as can be seen from the results of the Chi-squared test measuring the correlations between labels (Table 1). These multi-label methods were compared in terms of their predictive ability in the classification of various ABC transporters' substrates and non-substrates.

**Table 1**. Values of the Chi-squared test measuring correlation between labels. The smaller the Chi-squared value, the stronger the change of true correlation.

| | MDR1 | MRP1 | MRP2 |
|---|---|---|---|
| **BCRP1** | 0.001 | 0.001 | <0.001 |
| **MDR1** | | <0.001 | 0.679 |
| **MRP1** | | | <0.001 |

Within each multi-label model it is necessary to make sure that each one of its single-label models provides a reasonable input to the global multi-label model. Firstly, we selected the best single-label J48 model for each transporter out of a pool of five models obtained from various pre-processing feature selection methods. The results showed that the GS method led to the best model for BCPR1, while J48-GA led to the best models for MDR1 and MRP1; and ReliefF led to the best model for MRP2 (Supporting Information SI 1). Table 2 shows the performance of the best single-label models.

Secondly, to validate the inclusion of each label, the impact of removing a label or the addition of new labels on the overall performance of BR and CC models, respectively, was assessed by HL, with respect to the IV set (Figure 3). Both BR and CC models show a constant impact in HL by the presence of all labels, which is depicted by a constant HL value as the chain grows, in CC, and when different labels are removed in turn, in BR (Figure 3). This observation justifies the presence of each label in the multi-label models. The same is observed in the TE set where no particular label stood out in terms of impact on HL performance (Figure 4) which means no label is causing degradation of the predictive performance.

**Table 2.** Test set (TE) performance of the single-label models for individual transporters using the best set of features with (CC) or without (BR) the use of the predicted ABC binding class of the preceding transporters in the classifier chain.

| | MDR1 | BCRP1 | | MRP2 | | MRP1 | |
|---|---|---|---|---|---|---|---|
| | (n=195) | (n=87) | | (n=41) | | (n=36) | |
| | J48-GA | GS | GS pMDR1 | RfF | RfF pMDR1 pBCRP1 | J48-GA | J48-GA pMDR1 pBCRP1 pMRP2 |
| G-mean | 66.8 | 76.3 | **76.7** | 74.4 | 74.4 | 58.9 | **59.0** |
| SEN | 79.1 | 84.5% | 77.6 | 69.2 | 69.2 | 84.2 | 74.0 |
| SPE | 56.5 | 69.0% | 75.9 | 80.0 | 80.0 | 41.2 | 47.1 |
| MCC | 36.6 | 53.4% | 51.4 | 47.4 | 47.4 | 28.3 | 21.6 |

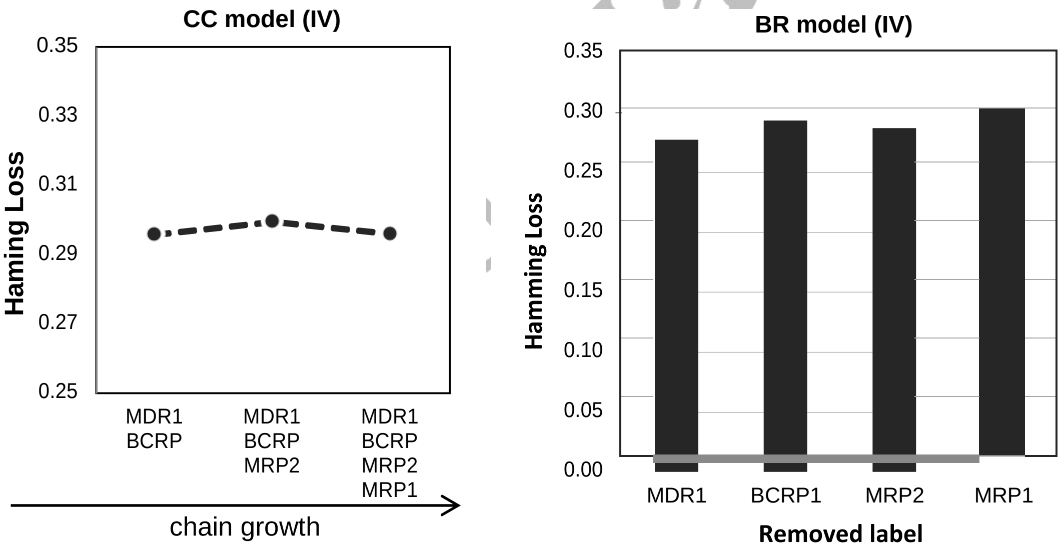

**Figure 3.** Impact of each label on the overall performance of the CC and BR models, tested on the IV set. The graph for CC depicts the evolution of the model's performance as labels are being added to the chain, whereas the graph for BR depicts the model's performance when each of the labels is removed, in turn.

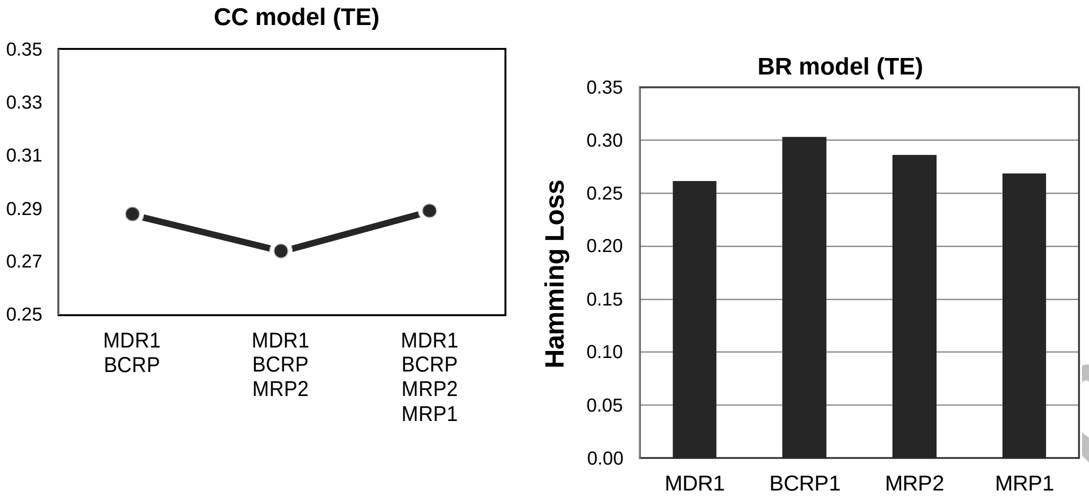

**Figure 4.** Impact of each label on the overall predictive TE performance of the CC and BR models. The graph for CC depicts the evolution of the model's performance as labels are being added to the chain, whereas the graph for BR depicts the model's performance when each of the labels is removed, in turn.

At the multi-label level, Table 3 indicates a good performance with an overall F1 of approximately 70% for both BR and CC models. The results also show that both models performed very similarly, however attention must be drawn to the fact that the modelled data is imbalanced both at the label level (i.e. some transporters have more data than others) and at the class level (i.e. within each transporter there is more substrates than non-substrates). This means that commonly employed measures, such as F1, precision and recall, will be leveraged by the majority label and the majority class, and therefore they are not ideal to assess these imbalanced problems. Alternatively, bACC has been designed to overcome this issue. Table 3 shows that bACC has a higher score for CC. Additionally the CC model shows less discrepancy between the ability to predict substrates and non- substrates, shown by the absolute difference between both with regard to precision and recall (ΔPR). This means the CC model achieves the best balance in terms of classifying both substrates and non-substrates. Moreover, a comparison of single-label (individual transporter) models used to develop BR and CC (Table 2) shows that the two single-label models that include a predicted label as a feature (BCRP1, and MRP1) have improved SEN-to-SPE balance, which supports the existence of label correlations and the advantage of taking them into account when modelling ABC transport data by using CC instead of BR.

**Table 3.** Summary of performance measures of the final BR and CC models in the test set. Underlined font marks the values that are better than their direct counterpart models.

| Performance measures | BR | CC |
|---|---|---|
| **F1** | 69.6 % | 69.2 % |
| **bACC** | 68.7 % | 69.0 % |
| **Precision** | 70.4 % | 70.0 % |
| **Recall** | 70.0 % | 69.6 % |
| **ΔPR** | 20.6 % | 17.4 % |

### 3.2 Molecular descriptors in single-label elements of BR and CC

As it was explained in previous sections, the molecular descriptors used in J48 models have been selected by the best pre-processing feature selection methods for each transporter dataset followed by the embedded J48 feature selection. Roughly the same number of molecular descriptors was provided to the J48 algorithm for the modelling of each transporter, however the number of descriptors used to build each tree decreased along the order of the labels in the chain, i.e. MDR1, BCRP1, MRP2, and MRP1. Moreover, recall that the same set of molecular descriptors was provided to J48 for the single-label constituents of the BR and CC models, but single-label elements of CC employ additional predictors, i.e. the predicted substrate class of the previous transporter(s) in the chain.

Molecular descriptors used in single-label J48 models have been presented in the Supporting information SI 2 in the form of a series of IF-THEN rules. These have been automatically compiled from the tree in Weka's output using a python script and can be easily implemented for further use. Given the large number of molecular descriptors incorporated in some J48 models, these descriptors can be ranked according to the statistical importance and the most important molecular descriptors may be identified. Tables 4 and 5 show the importance of molecular descriptors in J48 models for different transporters in BR and CC models, respectively. These molecular descriptors have been described in Supporting Information SI 3. In order to calculate the feature importance, the molecular descriptors used in the models were ranked according to the number of compounds that were directly affected by each descriptor at any point of the tree. In this way, descriptors selected earlier on for major branches of trees are more important than those selected later on to classify a smaller number of compounds. Table 5 shows that the molecular descriptors selected by J48 algorithm for BCRP1 and MRP1 include a transporter substrate class predicted by the previous transporters in the chain, and both predicted labels used in both models affected more than 50% of the training data (see Table 5).

Due to the design of the CC model that placed MDR1 model as the first label, the single-label MDR1 model used in both multi-label BR and CC models is the same, i.e. no predicted ABC label was used as a feature in the modelling of this transporter. As a result MDR1 descriptors reported in Tables 4 and 5 are the same. For BCRP1, a comparison of Tables 4 and 5 shows that some of the molecular descriptors in the BR model have been replaced by the predicted MDR1 class as an important feature in the CC model of BCRP1. On the other hand, the single label MRP2 model developed by J48 did not pick predicted MDR1 or predicted BCRP1 labels, and only molecular descriptors were selected as the model features. As a result, the top descriptors used in the single label MRP2 models within both BR and CC models are the same (see Table 4 and 5). For MRP1 models, a comparison of Tables 4 and 5 shows that the models developed for CC and BR are different, as the predicted MRP2 labels have been used in the multi-label MRP1 model built by the CC model. The MRP1 model for CC used the predicted MRP2 label as the second most important feature replacing the polar volume.

**Table 4.** Descriptor importance calculated from the relative amount (%N) of compounds classified using every given feature within the BR model. See Supporting Information SI 4 for descriptor definitions.

| MDR1 | %N | BCRP1 | %N | MRP2 | %N | MRP1 | %N |
|---|---|---|---|---|---|---|---|
| (J48-GA) | | (GS) | | (RfF) | | (J48-GA) | |
| **VDistMa** | 100 | Num_Rings_4 | 100 | ast_violation_ext | 100 | Q_VSA_POL | 100 |
| **FCharge** | 85 | Q_VSA_FPPOS | 94 | PEOE_VSA_FPNEG | 65 | vsurf_Wp1 | 70 |
| **a_nH** | 80 | SlogP_VSA7 | 82 | vsurf_CW2 | 61 | Q_VSA_FPPOS | 53 |
| **b_max1len** | 64 | b_ar | 68 | reactive | 54 | FCASA+ | 38 |
| **PM3_LUMO** | 63 | opr_nring | 53 | Fi(B) | 34 | chi1v_C | 34 |
| **PEOE_VSA+6** | 52 | a_nF | 30 | b_rotR | 24 | b_rotR | 30 |
| **SMR_VSA2** | 45 | glob | 24 | opr_leadlike | 16 | b_max1len | 15 |
| **a_acc** | 27 | a_ICM | 23 | Q_VSA_FHYD | 12 | Kier3 | 14 |
| **b_ar** | 25 | PEOE_VSA-3 | 22 | vsurf_HB2 | 11 | | |
| **dens** | 22 | LogD(6.5) | 19 | Fi(A) | 4 | | |
| **PEOE_VSA-6** | 20 | MNDO_LUMO | 18 | | | | |
| **Num_Rings_5** | 16 | SMR_VSA4 | 9 | | | | |
| **FCASA-** | 13 | LogD(5.5) | 5 | | | | |
| **vsurf_Wp5** | 11 | PEOE_VSA-4 | 3 | | | | |
| **vsurf_Wp6** | 10 | PEOE_VSA-1 | 2 | | | | |
| **SlogP** | 8 | vsurf_R | 2 | | | | |
| **Rule_Of_5** | 8 | LogD(7.4) | 2 | | | | |
| **PM3_E** | 8 | | | | | | |
| **MW** | 3 | | | | | | |
| **vsurf_CW8** | 2 | | | | | | |
| **PEOE_VSA_NEG** | 2 | | | | | | |
| **Polarizability** | 2 | | | | | | |

**Table 5.** Descriptor importance calculated from the amount of compounds classified using every given feature within the CC model.

| MDR1<br>(J48-GA) | %N | BCRP1<br>(GS) | %N | MRP2<br>(RfF) | %N | MRP1<br>(J48-GA) | %N |
|---|---|---|---|---|---|---|---|
| **VDistMa** | 100 | Num_Rings_4 | 100 | ast_violation_ext | 100 | Q_VSA_POL | 100 |
| **FCharge** | 85 | Q_VSA_FPPOS | 94 | PEOE_VSA_FPNEG | 65 | pMRP2_RfF | 70 |
| **a_nH** | 80 | SlogP_VSA7 | 82 | vsurf_CW2 | 61 | vsurf_D7 | 46 |
| **b_max1len** | 64 | b_ar | 62 | reactive | 54 | b_rotR | 30 |
| **PM3_LUMO** | 63 | pMDR1_J48-GA | 55 | Fi(B) | 34 | Q_VSA_FPPOS | 24 |
| **PEOE_VSA+6** | 52 | opr_nring | 48 | b_rotR | 24 | rings | 17 |
| **SMR_VSA2** | 45 | glob | 46 | Q_VSA_FHYD | 12 | b_max1len | 14 |
| **a_acc** | 27 | a_nF | 30 | vsurf_HB2 | 11 | | |
| **b_ar** | 25 | PEOE_VSA-3 | 22 | | | | |
| **dens** | 22 | MNDO_LUMO | 21 | | | | |
| **PEOE_VSA-6** | 20 | vsurf_CW2 | 19 | | | | |
| **Num_Rings_5** | 16 | LogD(6.5) | 19 | | | | |
| **FCASA-** | 13 | a_ICM | 9 | | | | |
| **vsurf_Wp5** | 11 | LogD(5.5) | 7 | | | | |
| **vsurf_Wp6** | 10 | SMR_VSA4 | 7 | | | | |
| **SlogP** | 8 | a_aro | 4 | | | | |
| **Rule_Of_5** | 8 | PEOE_VSA-4 | 3 | | | | |
| **PM3_E** | 8 | vsurf_R | 2 | | | | |
| **MW** | 3 | LogD(7.4) | 2 | | | | |
| **vsurf_CW8** | 2 | | | | | | |
| **PEOE_VSA_NEG** | 2 | | | | | | |
| **Polarizability** | 2 | | | | | | |

### 3.3 Applicability Domain and Activity Cliffs

Applying the STD method as per Sushko et al.[25], it is possible to observe an overall declining trend of accuracy vs STD across the majority of the single-label models (Figure 5). Exceptions to this trend will be further explored.

There are two main important aspects to consider for the quality of an AD profile, similarity of overall profiles/trends for the subsets of data and a decreasing accuracy as the chemical space moves away from the model's core. Exploring Figure 5 points to only two cases where the requirements above have not been met; these are MDR1-BR and MRP2-BR in the IV set. This is not seen for the corresponding CC model MRP2-CC (note that MDR1 single-label model is same in both BR and CC models). There is also a mild case of disparity between IV and TE for BCRP1 (although only at the first iteration of STD increments). While this disparity happens for BR, in the CC model all trends start in a higher point and tend to decrease with STD (although this is not done in a perfectly smooth way, as expected from any kind of AD analysis).

Interestingly, even though MRP2 models show the exact same performance statistics at the single-label level (Table 2), there is a marked difference between the applicability domain profiles of its BR and CC single-label models developed using a 10-fold bagging ensemble, depicted in Figure 5.

Lastly, it should be noted that, for some labels, the increase in accuracy is not significant for smaller STD values. This is due to the quality of the trained model that may not allow a high level of precision (agreement between the ensemble models). Still, even if there is a small gain in accuracy at a given threshold, this still entails a decreased risk of producing a wrong prediction, and thus the respective AD profile is useful in guiding the prediction acceptance.

Even though this analysis gives insight to a model's overall performance across the data, it is convenient to further pinpoint activity cliff regions. Table 6 shows that a considerable portion of activity cliffs coincides with mispredictions. These can be areas of higher complexity in terms of the structure-property relationship that require more compounds and/or better use of molecular descriptors that would capture that subtle chemical variation.[32] These can also result from unreliable experimental data (i.e., if a substrate is incorrectly presented to the learning algorithm as a non-substrate, even if it is correctly predicted as substrate it will be perceived as a misprediction).[33]

Recall that three single-label models in the multi-label classifier chain could use previous labels as descriptors (considering that MDR1, as the first label of the chain, cannot use previous label descriptors). The fact that in two out of those three models a considerable portion of the activity cliffs was associated with mispredictions shows the correlation between both. It should be pointed out that in both BCRP1 models (produced by the BR and CC methods) there were two compounds that were mispredicted in the former model while being correctly predicted in the latter.

T**able 6**. Comparison between Activity cliffs (ACs) and mispredictions within them – values in brackets are the percentage of activity cliff compounds that are mispredicted by the models.

| Transporter | Number of ACs mispredicted | Number of ACs |
|---|---|---|
| MDR1 (BR/CC) | 9 (50%) | 18 |
| BCRP1 (BR &CC) | 4 (40%) | 10 |
| MRP1 (BR & CC) | 2 (100%) | 2 |
| MRP2 (BR & CC) | 0 | 2 |

As an example, Figure 6 depicts the distribution of mispredictions (FN and FP) for the BCRP1 BR model overlaid with the substrates and non-substrates. It can be seen that activity cliffs are mainly located in areas of sparse data especially at the extremities of the plot.

Mispredictions were further analyzed for their distribution along the TE set chemical span of each of the molecular descriptors used in the various decision trees (all distribution graphs are shown in Supporting Information SI 5). For all models in BR and CC, mispredictions overlap with correct predictions in the TE set. Furthermore, it is common to find both mispredicted compounds close to the center-values, and correctly predicted compounds near data limits (and even outside the training range).

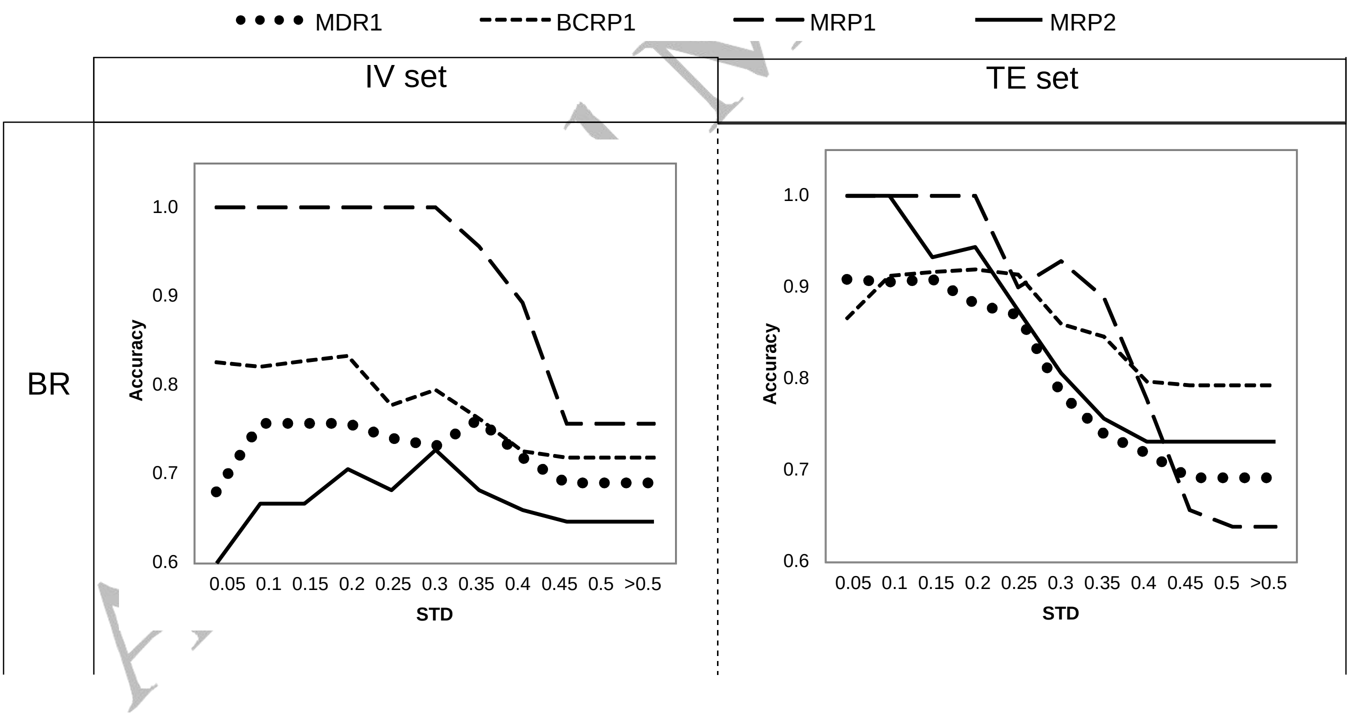

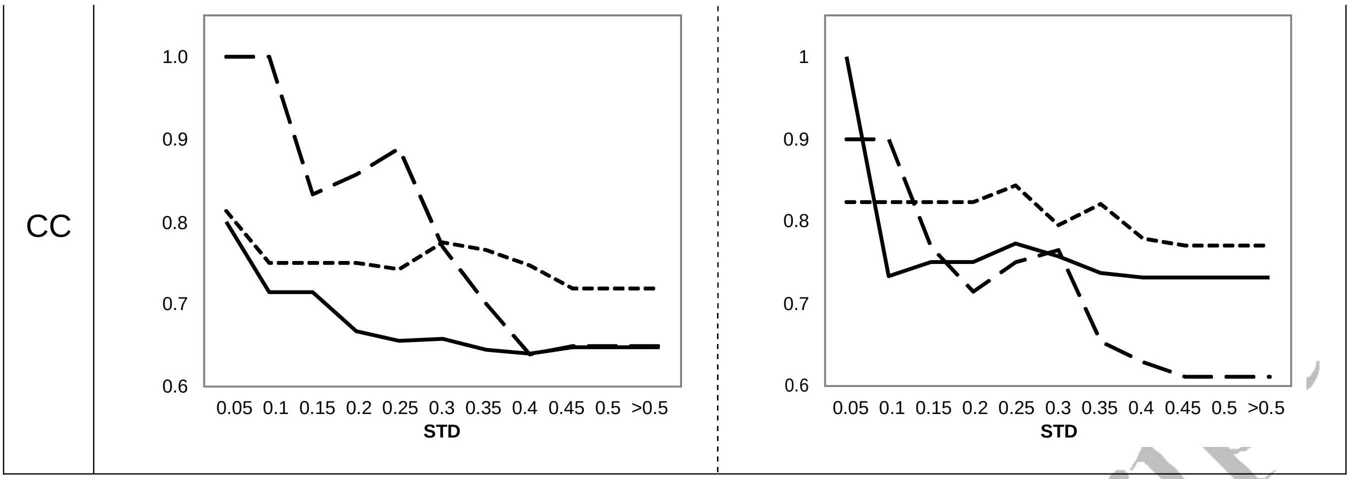

**Figure 5.** Applicability domain evaluated with respect to the IV and TE sets. Recall that accuracy has been defined as the % correct predictions out of the total amount of predictions that fall within any given threshold (set in the axis labeled "STD").

The IV and TE were also analyzed for their distribution with respect to the TR chemical span. This revealed no apparent trend in terms of misprediction concentration in chemical space, with the mispredicted compounds often showing scattering centered at the median of each descriptor. As a matter of fact, mispredicted cases seem to follow the distribution of the training set, being more densely located near the median and scattering away from it in a somewhat parallel manner. Additionally, both in MDR1 and BCRP1 datasets, despite some compounds being clear outliers with respect to certain individual descriptors, as seen in Supporting Information SI 4, falling outside the maximum range of the training set ([0;1], standardized data) they were successfully predicted by their respective models. However, these observations were exceptions and, overall, the IV sets were found within the maximum range of each descriptor in the training set.

Apart from the applicability domain and activity cliff analysis, it is useful to analyze the range of chemical diversity covered by the models built, in order to support the validity of their future predictions. We achieved this by overlaying our datasets with the DrugBank dataset using a t-SNE multidimentional scalling projection of the Euclidean distances (Figure 7). Considering that DrugBank holds the full span of chemical variety in real-world drug space, this analysis provides a gauge of the diversity of our data. Despite the scarcity of data in some transporter datasets they were all evenly spread across the chemical space of the entire DrugBank dataset (more than 6000 instances). This means that the models incorporate a wide chemical variety in the training, which strengthens their potential usefulness as a predictive tool.

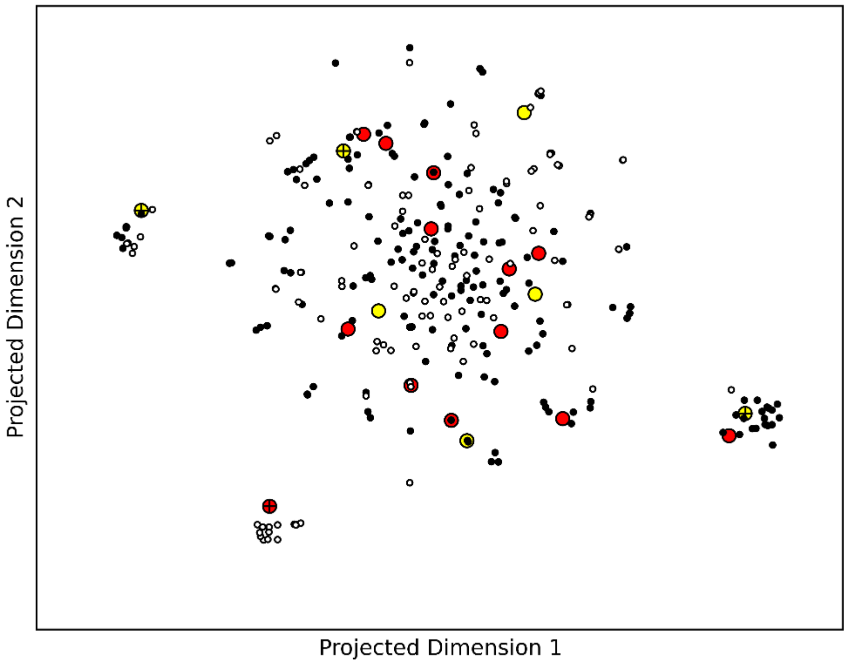

**Figure 6.** Mispredictions and activity cliffs of the BCRP1-BR model; Training data were projected into a 2D map using t-SNE, and the location reflects the Euclidean distance between ECFP4 fingerprints. The Tc coefficient was not used as a visualization measure as it produces plots with very distant points. However, using the Euclidean distance conserves visually the relative neighborhood of each point. Activity Cliffs are marked with a cross; FP: yellow; FN: red; training substrates: black; training non-substrates: white.

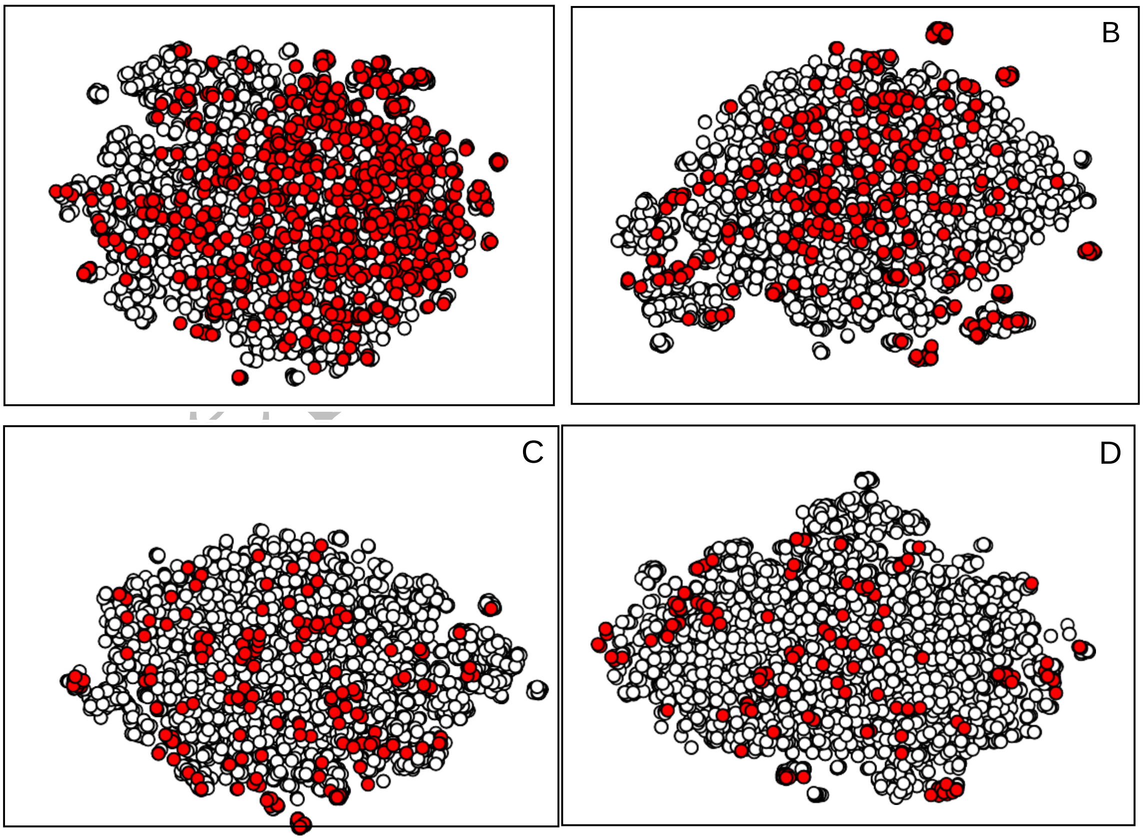

**Figure 7.** Chemical space coverage of MDR1/P-gp (A), BCRP1 (B), MRP2 (C) and MRP1 (D) with respect to the DrugBank complete dataset. The ABC datasets are represented in red in their respective scatterplots, and DrugBank data is depicted in white. The plots result from a t-SNE multidimentional scalling projection of the Euclidean distance calculated from ECFP4 fingerprints.

# 4 Discussion

### 4.1 Multi-label QSAR models

In this work we sought out to build multi-label models using a decision tree learner to predict compounds binding to several ABC transporters as substrates. The main advantage of using decision trees to build a predictive model is that their visual and transparent nature allows interpretation of the effects of the features on the predicted labels. Furthermore, decision trees can cope with different scales in the descriptors and they can also handle both continuous and categorical data efficiently and robustly.[34] In order to test whether there is a correlation between the binding profiles of different ABCs, two types of multi-label models (BR and CC) differing only in the ability to address overlap between labels were implemented in the modeling of ABC substrate recognition. Despite the substrate overlap between various members of the ABC transporters [38, 39], BR and CC yielded very similar predictive performance statistics. On the other hand, it is apparent that the predicted MDR1 class is favored over molecular descriptors in the BCRP1 model, and the predicted MRP2 class is preferred in the MRP1 model, as evidenced by the preferential selection of these features as one of the top five model features (compare BR and CC features in Table 4 and Table 5). There are several possible explanations for the lack of a significant improvement of CC comparatively to BR (Table 3). The first explanation may be that labels have close to no interaction, which means that the classifier chain has nothing to capitalize from. However, Table 1 shows that all pairs of labels, except one, have a significant correlation, so the issue with regard to this hypothesis may be the relatively low label density (the compound vs label matrix is only 23% populated in the training set), which reveals scarcity of multi-label cases (i.e., compounds with measured binding in several transporter systems). The second explanation may be due to the fact that the BR model depends on the individual quality of each single-label model; while the quality of the CC model depends also on the quality of the prediction of the previous labels in the chain. In fact, in a CC model every flaw in any given label (transporter) will be carried on to the following labels in the chain, as opposed to BR, in which the shortcomings of a model have no effect on the remaining labels.

Even though the final overall statistics show no marked improvement from accounting for label interaction, focusing only on this can give an overly simplistic view. When results are analyzed as a whole, there are several evidences of the value of using label interaction in the modelling of the ABC QSAR. In two of the three single-label models, built by the CC method, where previous labels were available, previous label information was spontaneously selected by the tree building algorithm. Furthermore, this singular change in the entire modelling process coincided with more parsimonious models, which showed more balanced SEN to SPE ratio. This is a very valuable improvement given that this modelling task would naturally tend towards higher SEN, brought on by an imbalance in the data (high ratio of substrates to non-substrates). Data imbalance is known to have yielded poor models in the past[33, 35], and being able to mitigate this issue without using any type of aiding technique (i.e., over-/under-sampling or misclassification cost) is notable. Lastly, the presence of previous labels allowed establishing a more reliable AD of the model. This is observed with MRP2 models, where even though both MRP2-CC and MRP2-BR yielded equal predictive performance, MRP2-CC allows a better definition of its applicability as both external datasets show the same trend of accuracy vs STD (Figure 5). As the AD method is insensitive to bias and relies solely on precision, low STD scores may happen due to a systematic misprediction in all models in the ensemble rather than a reliable (correct) prediction. This systematic misprediction in low STD area was the case in MRP2-BR. On the other hand, the presence of two extra features in MRP2-CC (the two previous labels in the chain), which were picked for 3 of the 10 bagged models, helped overcome the systematic bias in modelling MRP2 data. Therefore, MRP2-CC allows establishing a threshold of prediction reliability that imitates the reliability trend in external data. As a result, these observations consist of a proof of concept of the value of using CC for the purpose of modelling ABC substrate data.

Activity cliff analysis was used in this study to identify areas of high complexity in the structure-activity data. There was a high incidence of mispredictions in the activity cliff areas.

An analysis of outliers showed a lack of correlation between location in descriptor span and misprediction. This is an indication that the misprediction rate appears to have no connection with the descriptor span coverage by the model.

The performance of our models has to be evaluated in light of the high level of noise in any kind of large transporter dataset. Several factors are known to contribute to the considerable inter-laboratory and even inter-experimental variability in permeability/efflux assays. Some frequently reported examples are sensitivity to varied culture protocols and conditions, genetic change of MDR1 (and other transporters) leading to variable pump functionality, and variable expression levels of various ABC transporters and even different additional transporters (i.e. Solute Carriers).[[36-37] There are also parallel metabolizing enzymes and alternative active transport systems. The variability is therefore a significant factor within a single dataset built from different sources using different cell models.[38] As a result, the BR and CC models should be evaluated in light of realistic maximum obtainable performance. In an ideal scenario a perfect model would correctly classify 100% of unambiguous cases (correctly belonging to their assigned classes), and would correctly classify 50% of ambiguous cases (given that probabilistically only 50% are actually correctly classified to begin with). Applying this reasoning to our dataset translates into a maximum accuracy of 98% since our dataset has 61 ambiguous responses (i.e. reported as substrate and non-substrate from different sources) across 1493 compounds, hence 2% will theoretically be mispredicted. However this is a conservative estimate, due to the inter-laboratory variations affecting the accuracy of a given label in the literature, where the majority of compounds in the dataset have only one experimental measurement**.** It must be noted that in the construction of Metrabase, the allocation of substrate and non-substrate labels was carried based solely on the recommendation of the original literature reference.[12] However different literature sources have differing criteria and threshold values (in addition to varying experimental techniques) for classifying a compound as substrate.[39] A threshold of 2 for the efflux ratio is normally used by researchers, while the borderline interval is [1.8-2.5].[39] In fact a maximum accuracy of 86% has been reported for MDR1 efflux assays.[39] In an overall appreciation of the feasibility of using the models presented here, as a substitute of the gold standard cell assays, these models are able to produce valid predictions in 70% of the cases while the Borst cell assay (n=91, see Broccatelli et al.[39]) produced usable prediction in 76% of the cases considering that contradictory replicates (n=16) and borderline values (n=6) cannot be used to trustfully classify a given compound.

In this study, even for models that were trained on datasets with balanced classes, the specificity is always considerably lower than the sensitivity, which means that the models are generally more capable of identifying substrates than non-substrates. However, this is not unprecedented as several other works on MDR1 substrate prediction listed in the literature[39] have reported the same issue. Comparing the results of two previous works where efflux ratios of 2[39] vs 2.5[40] have been used as threshold values, models with higher threshold values generally lead to lower specificity as expected. It can be hypothesized that the main underlying cause for a tendency for poor SPE is the fact that some substrates also have high passive permeability. This leads to cases of substrates that cannot be identified by permeability measurement methods (false non-substrates), which will translate into spurious data in the non-substrate class.[39]

To contextualize the potential utility of the CC model proposed here, as of 2012, Tsaioun and Kates[41] reported a 15% increase in phase 2 failures, 50% of which are due to lack of efficacy. However, many of these failures are CNS-targeted clinical trials where lack of efficacy is caused by an underlying failure to permeate the blood brain barrier (BBB). It is safe to say that, considering the polyspecificity of MDR1 in addition to the presence of a large variety of other ABC exporters on the BBB, a large portion of this attrition rate could probably be associated to some extent with the efflux of the drugs in question. In fact, in retrospect it is possible to identify cases where, if our models had been used, it would have been possible to avoid very expensive clinical trials through the prediction of the substrate ability of different ABC substrates. Two examples from our test set are sunitinib and dasatinib, both predicted as MDR1 and BCRP1 substrates based on our CC and BR models. Sunitinib failed a phase II clinical trial (NCT00923117) for the treatment of glioblastoma due to lack of efficacy. The probable cause for such late failure was that this drug has poor ability to permeate the BBB, which is most likely due to MDR1 and BCRP1 efflux.[42]
In retrospect, if the models herein developed had been applied to sunitinib, it would be possible to avoid a failed clinical trial since both BR and CC were able to predict this compound as a substrate of both transporters. Even if the trial was carried out, the use of a predictive model like ours would at the least maximize the chances of success with the concomitant administration of an inhibitor. A similar scenario was observed for dasatinib, which showed no effectivity in a clinical study with 14 patients.[43]

### 4.2 Molecular descriptors in the single-label elements of the models

In this investigation we used five pre-processing wrapper methods to find the best set of molecular descriptors that can produce the most accurate J48 models for the prediction of each of the four labels (transporters' substrates/non-substrates). Among the five feature selection methods, J48-GA features yielded the best results for the majority of single-label models. The purpose of using a wrapper rather than a filter method is to select a feature set that ideally best copes with the classification algorithm's biases. However, given the complex nature of these transporters it is expected that different feature-selection methods are best suited for the predictions of different labels, and indeed this has been observed in our results.
Common features between transporters could be an indication of the degree of shared substrates. MDR1 and MRP1 both share the same best feature selection method (J48-GA) and there is some degree of feature overlap (around 5 features) between them. MDR1 shows the strongest correlation with MRP1 (Chi-squared test, $p < 0.001$, Table 1), and in fact there is a considerable amount of common substrates and non-substrates between them (n=34 and n=12, respectively out of 61 common compounds). The overlap of substrates between various ABC transporters is a well-established phenomenon.[44] For instance, it was reported that drug resistance to daunorubicin derives from a synergy between MRP1 and MDR1 activities.[45]

The nature of the molecular descriptors incorporated into the single label J48 models can be interpreted in order to identify the molecular characteristics leading to a compound being recognized by a transporter as its substrate (See the Supporting Information Table SI 3).

## 5 Conclusions

In conclusion, this work reports two multi-label models for the prediction of various ABC transporter substrates and non-substrates, namely BCRP1, MDR1/P-gp, MRP1 and MRP2. The multi-label classifier chain method, which accounts for label (transporter) interaction, was compared with the binary relevance method, which does not consider interaction. Both models showed good predictive power, as expressed by F1 values (weighted average of precision and recall) and a balanced accuracy of approximately 70%. Even though the CC model showed no marked improvement in terms of the general performance measures, a closer analysis revealed several evidences of the benefit of taking into account label interaction. Firstly, despite the natural tendency for a relatively poorer ability to classify non-substrates (as they are the minority class, and are also more prone to containing noisy data), the CC model showed more balanced single-label models that compromised slightly on SEN (sensitivity) to gain some SPE (specificity). This translates into a lower ΔPR measure (average deviation in precision and recall) for the CC model, indicative of less discrepancy between the ability to predict substrates and non-substrates. Secondly, two of the single-label models used other predicted labels in preference to the molecular descriptors during the CC training, leading to improved SEN to SPE balance. Thirdly, the two MRP2 single-label models within CC and BR, despite showing the same predictive accuracy performance, resulted in two very different applicability domain profiles. While MRP2-CC allowed establishing a more reliable accuracy vs STD profile, which emulates more closely the reliability profile in external data, MRP2-BR was not able to achieve this. We hypothesize the presence of previous label predictions allowed overcoming a systematic bias in the ensemble predictions, as this is the only aspect that changed between BR and CC. These observations consist of a proof of concept of the utility of addressing transporter overlap when modelling a QSAR, and possibly more marked effects could be obtained with a more populated matrix of instances vs transporters.

An analysis of the molecular features showed that there is some degree of overlap between transporters in terms of the molecular features responsible for substrate recognition, which supports the multi-label approach from a mechanistic standpoint. In particular, features of MDR1 and BCRP1 substrates have some similarity as both transporter's substrates are bulky and flexible, and contain hydrophobic moieties. MDR1 substrates are highly branched, good electron acceptors (such as in hydrogen bonds) and contain quaternary ammoniums, while BCRP1 substrates contain large positively charged surface, have aromatic rings and may be a non-drug-like molecule. The correlation of these two transporters is evidenced by the fact that the predicted MDR1 label is a very useful feature for the classification of BCRP1 transport. On the other hand, molecular features of MRP2 and MRP1 substrates are also similar in terms of polarity and hydrophilicity of the molecular surface. MRP2 substrates may contain reactive groups defined as nitrogen, oxygen and sulfur atoms with polar negative surface area, while MRP2 substrates are flexible in addition to large polar and hydrophilic surface area. Furthermore, the predicted MRP2 binding class can be used as a significant feature for the prediction of MRP1 transport. MDR1 and BCRP1 were more associated with explicit aromaticity-related features, whereas MRP1 and MRP2 where predominately more associated with hydrophilicity-related properties, which could be tied with the fact that MDR1 and MRP2 were used as predictors in both BCRP1 and MRP1 models respectively.

Overall, the models revealed to be robust and of acceptable predictive performance, especially considering the complexity of trying to uncover unspecific mechanisms of substrates recognition by the ABC family members.

## References

[1] M. Pinto, D. Digles, G. F. Ecker, *Drug Discovery Today: Technol.* 2014, *12*, e69-77.

[2] B. Marquez, V. Bambeke, *Curr. Drug. Targets.* 2011, *12*, 600-620.

[3] G. Szakács, A. Váradi, C. Ozvegy-Laczka, B. Sarkadi, *Drug discovery today* 2008, *13*, 379-393.

[4] M. Demel, O. Kraemer, P. Ettmayer, E. Haaksma, G. Ecker, *Molecular Informatics* 2010, *29*, 233-242.

[5] P. V. Desai, G. A. Sawada, I. A. Watson, T. J. Raub, *Mol. Pharm.* 2013, *10*, 1249-1261.

[6] N. S. Wind, I. Holen, *Int. J. Breast Cancer* 2011, *2011*, 967419.

[7] M. L. Zhang, Z. H. Zhou, in *IEEE Transactions on Knowledge and Data Engineering, Vol. 26*, 2014, pp. 1819-1837.

[8] O. Luaces, J. Díez, J. Barranquero, J. del Coz, A. Bahamonde, *Progress in Artificial Intelligence* 2012, *1*, 303-313.

[9] E. Gibaja, S. Ventura, *Wiley Interdisciplinary Reviews: Data Mining and Knowledge Discovery* 2014, *4*, 411-444.

[10] J. Read, B. Pfahringer, G. Holmes, E. Frank, in *Machine Learning and Knowledge Discovery in Databases SE - 17, Vol. 5782* (Eds.: W. Buntine, M. Grobelnik, D. Mladenić, J. Shawe-Taylor), Springer Berlin Heidelberg, 2009, pp. 254-269.

[11] F. Montanari, B. Zdrazil, D. Digles, G. F. Ecker, *J. Cheminf.* 2016, *8*, 7.

[12] L. Mak, D. Marcus, A. Howlett, G. Yarova, G. Duchateau, W. Klaffke, A. Bender, R. Glen, *J. Cheminf.* 2015, *7*, 31.

[13] K. Sechidis, G. Tsoumakas, I. Vlahavas, in *ECML PKDD 2011, Vol. 3* (Eds.: D. Gunopulos, T. Hofmann, D. Malerba, M. Vazirgiannis), Springer, Greece, 2011, pp. 145-158.

[14] J. J. P. Stewart, Stewart Computational Chemistry, Colorado Springs, USA, 2009.

[15] R. R. Mittal, L. Harris, R. A. Mckinnon, M. J. Sorich, *J. Chem. Inf. Model.* 2009, *49*, 704-709.

[16] V. Bolón-Canedo, N. Sánchez-Maroño, A. Alonso-Betanzos, *Knowl Inf Syst* 2013, *34*, 483-519.

[17] Y. Saeys, I. Inza, P. Larrañaga, *Bioinformatics* 2007, *23*, 2507-2517.

[18] N. Spolaôr, E. A. Cherman, M. C. Monard, H. D. Lee, *Electron Notes Theor Comput Sci* 2013, *292*, 135-151.

[19] M. Shahlaei, *Chemical Reviews* 2013, *113*, 8093-8103.

[20] L. Eriksson, J. Jaworska, A. P. Worth, M. T. D. Cronin, R. M. McDowell, P. Gramatica, *Environ. Health Perspect.* 2003, *111*, 1361-1375.

[21] G. Tsoumakas, I. Katakis, *Int. J. Data Warehouse. Min.* 2007, *3*, 1-13.

[22] G. Tsoumakas, I. Katakis, I. Vlahavas, in *Data Mining and Knowledge Discovery Handbook* (Eds.: O. Maimon, L. Rokach), Springer, New York, 2010, pp. 667-685.

[23] Y. Sushko, S. Novotarskyi, R. Körner, J. Vogt, A. Abdelaziz, I. Tetko, *J. Cheminf.* 2014, *6*, 1-18.

[24] H. Dragos, M. Gilles, V. Alexandre, *J. Chem. Inf. Model.* 2009, *49*, 1762-1776.

[25] I. Sushko, S. Novotarskyi, R. Ko, A. K. Pandey, A. Cherkasov, H. Liu, X. Yao, O. Tomas, F. Hormozdiari, P. Dao, C. Sahinalp, R. Todeschini, P. Polishchuk, A. Artemenko, V. Kuz, T. M. Martin, D. M. Young, D. Fourches, E. Muratov, A. Tropsha, I. Baskin, D. Horvath, G. Marcou, C. Muller, A. Varnek, V. V. Prokopenko, I. V. Tetko, *J. Chem. Inf. Model.* 2010, *50*, 2094-2111.

[26] I. V. Tetko, I. Sushko, A. K. Pandey, H. Zhu, A. Tropsha, E. Papa, R. Todeschini, D. Fourches, A. Varnek, *J. Chem. Inf. Model.* 2008, *48*, 1733-1746.

[27] I. V. Tetko, S. Novotarskyi, I. Sushko, V. Ivanov, A. E. Petrenko, R. Dieden, F. Lebon, B. Mathieu, *J. Chem. Inf. Model.* 2013, *53*, 1990-2000.

[28] P. Iyer, D. Stumpfe, M. Vogt, J. Bajorath, G. M. Maggiora, *Molecular Informatics* 2013, *32*, 421-430.

[29] A. M. Wassermann, D. Dimova, J. Bajorath, *Chemical biology & drug design* 2011, *78*, 224-228.

[30] D. Stumpfe, J. Bajorath, *Journal of medicinal chemistry* 2012, *55*, 2932-2942.

[31] L. V. D. Maaten, G. Hinton, *Journal of Machine Learning Research* 2008, *9*, 2579-2605.

[32] G. M. Maggiora, *J. Chem. Inf. Model.* 2006, *46*, 1535.

[33] A. Sedykh, D. Fourches, J. Duan, O. Hucke, M. Garneau, H. Zhu, P. Bonneau, A. Tropsha, *Pharmaceutical research* 2013, *30*, 996-1007.

[34] M. Dehmer, K. Varmuza, in *Quantitative and Network Biology, Vol. 2*, 2012.

[35] D. Newby, A. A. Freitas, T. Ghafourian, *J. Chem. Inf. Model.* 2013, *53*, 461-474.

[36] S. Ganta, P. Sharma, S. Garg, in *Preclinical development handbook: ADME and Biopharmaceutical Properties* (Ed.: S. C. Gad), John Wiley and Sons, 2008.

[37] M. Vastag, E. Hellinger, M. L. Bakk, K. Tihanayi, *Ther. Delivery* 2011, *2*, 549-553.

[38] J. Bentz, M. P. O'Connor, D. Bednarczyk, J. Coleman, C. Lee, J. Palm, Y. A. Pak, E. S. Perloff, E. Reyner, P. Balimane, M. Brännström, X. Chu, C. Funk, A. Guo, I. Hanna, K. Herédi-Szabó, K. Hillgren, L. Li, E. Hollnack-Pusch, M. Jamei, X. Lin, A. K. Mason, S. Neuhoff, A. Patel, L. Podila, E. Plise, G. Rajaraman, L. Salphati, E. Sands, M. E. Taub, J.-S. Taur, D. Weitz, H. M. Wortelboer, C. Q. Xia, G. Xiao, J. Yabut, T. Yamagata, L. Zhang, H. Ellens, *Drug Metab. Dispos.* 2013, *41*, 1347-1366.

[39] F. Broccatelli, *J. Chem. Inf. Model.* 2012, *52*, 2462–2470.

[40] R. R. Gupta, E. M. Gifford, T. Liston, C. L. Waller, M. Hohman, B. A. Bunin, S. Ekins, *Drug Metab. Dispos.* 2010, *38*, 2083-2090.

[41] K. Tsaioun, S. A. Kates, in *Translational Stroke Research: From Target Selection to Clinical Trials* (Eds.: P. A. Lapchak, J. H. Zhang), Springer New York, New York, NY, 2012, pp. 617-638.

[42] R. K. Oberoi, R. K. Mittapalli, W. F. Elmquist, *J. Pharmacol. Exp. Ther.* 2013, *347*, 755-764.

[43] C. Lu-Emerson, a. D. Norden, J. Drappatz, E. C. Quant, R. Beroukhim, a. S. Ciampa, L. M. Doherty, D. C. Lafrankie, S. Ruland, P. Y. Wen, *Journal of neuro-oncology* 2011, *104*, 287-291.

[44] P. Matsson, J. Pedersen, U. Norinder, C. S. Bergström, P. Artursson, *Pharmaceutical research* 2009, *26*, 1816-1831.

[45] O. Legrand, G. Simonin, A. Beauchamp-Nicoud, R. Zittoun, J.-P. Marie, *Blood* 1999, *94*, 1046-1056.

[a] *Medway School of Pharmacy, Universities of Kent and Greenwich, Anson Building, Central Avenue, Chatham Maritime, Chatham, Kent ME4 4TB, UK*

[b] *School of Computing, University of Kent, Canterbury, Kent CT2 7NF, UK*

[c] *Centre for Molecular Science Informatics, Department of Chemistry, University of Cambridge, Lensfield Road, Cambridge CB2 1EW, UK*

[d] *School of Life Sciences, JMS Building, University of Sussex, Brighton, BN1 9QG, UK*
**e-mail: T.Ghafourian@sussex.ac.uk , phone/fax: +44(0)1273 678494*

*Supporting Information for this article is available on the WWW under www.molinf.com*